

Higher order glass-transition singularities in colloidal systems with attractive interactions.

K. Dawson¹, G. Foffi¹, M. Fuchs², W. Götze², F. Sciortino³, M. Sperl², P. Tartaglia³, Th. Voigtmann², E. Zaccarelli¹

¹*Irish Centre for Colloid Science and Biomaterials, University College Dublin, Belfield, Dublin 4, Ireland*

²*Physik-Department, Technische Universität München, D-85747 Garching, Germany*

³*Dipartimento di Fisica and Istituto Nazionale per la Fisica della Materia, Università di Roma La Sapienza, P.le A. Moro 2, I-00185 Roma, Italy*
(Phys. Rev. E, in print)

The transition from a liquid to a glass in colloidal suspensions of particles interacting through a hard core plus an attractive square-well potential is studied within the mode-coupling-theory framework. When the width of the attractive potential is much shorter than the hard-core diameter, a reentrant behavior of the liquid-glass line, and a glass-glass-transition line are found in the temperature-density plane of the model. For small well-width values, the glass-glass-transition line terminates in a third order bifurcation point, i.e. in a A_3 (cusp) singularity. On increasing the square-well width, the glass-glass line disappears, giving rise to a fourth order A_4 (swallow-tail) singularity at a critical well width. Close to the A_3 and A_4 singularities the decay of the density correlators shows stretching of huge dynamical windows, in particular logarithmic time dependence.

PACS numbers: 61.20.Ne, 64.70.Pf, 82.70.Dd

I. INTRODUCTION

Colloidal suspensions have been studied extensively because of their practical importance and because of their relevance in biophysics. These systems are also of great theoretical interest since they are models for conventional matter. They can be prepared for a large span of densities so that the states can be gases, gels, liquids, crystalline solids, or glasses. Light scattering can be used to measure the static structure factor and various correlation functions. The dynamics can be explored over a wide range of length scales and over huge dynamical windows [1,2]. Fascinating with colloidal systems is that the interaction can be tuned to some extent by varying the coating of the particles and the composition of the solvent [1–3]. It is possible to realize the hard-sphere system (HSS), the basic model underlying all theories of simple liquids [4,5]. One can also prepare systems where the hard core is complemented by an attractive shell. This allows to study the interplay of repulsion and attraction. As a contribution to such studies, a theory for the glass formation resulting from a strong short-range attraction among densely packed hard-sphere colloidal particles shall be presented in this paper.

In hard-sphere colloidal dispersions, the liquid-glass transition has been studied by van Meegen and Pusey

[6]. They measured correlation functions $\phi_q(t)$ for density fluctuations of a representative set of wave numbers q over about four decades in time t . It was found that these correlations decay to zero as expected for a liquid only for packing fractions φ below a critical value φ_c . At φ_c , the long-time limit of the correlators, $f_q = \phi_q(t \rightarrow \infty)$, changes discontinuously to a certain value $f_q^c > 0$, increasing further with packing fraction. f_q is the Debye-Waller factor of the amorphous solid, i.e. of the glass, and generalizes the order parameter introduced by Edwards and Anderson in the theory of spin glasses [7]. The evolution of the glassy dynamics for the HSS was studied comprehensively by van Meegen and coworkers [8–13]. The data suggest, that it is the well known cage effect [5] which causes the glassy dynamics and the arrest of density fluctuations at φ_c .

The cage effect is the essential physical concept underlying the mode-coupling theory (MCT) for the evolution of glassy dynamics in simple systems [14,15]. This theory allows the calculation of $\phi_q(t)$ and thus f_q from the equilibrium structure factor S_q . As a function of control parameters like φ , singularities of f_q , called glass-transition singularities, may occur. The simplest type, called a fold bifurcation, describes a liquid-glass transition at $\varphi = \varphi_c$. It implies a subtle dynamical scenario, giving rise to universal features of glassy dynamics, which have been identified in a leading-order-asymptotic expansion of the MCT equations. A review of the basic results is given in Ref. [16]. In Refs. [8–12], detailed quantitative comparisons of the data for hard-sphere colloids with the MCT predictions are presented. It is shown that the theory accounts for the experimental facts within a 15%-accuracy level. An illuminating summary of these studies is given in Ref. [17]. Results for the shear modulus have also been interpreted with the universal MCT formulas [18]. The evolution of glassy dynamics for φ increasing towards φ_c was also studied for polymer micronetwork colloids [19–22]. Here, the interparticle interaction is not known. But the authors demonstrated, that a consistent fit of their data with the universal MCT formulas was possible. Preliminary studies of the glassy dynamics of charge-stabilized colloids indicate, that these data can also be explained within MCT [23]. The reported findings shall be taken as a justification to base the theory in this paper on the MCT for simple systems.

Our studies deal with the square-well system (SWS), characterized by a hard-core repulsion for interparticle distances $r < d$, and by a constant attraction potential within the shell $d < r < d + \Delta$. The theory focuses on the high-density regime, say $\varphi > 0.4$, so that the cage effect is essential for the dynamics. The relative attraction-shell width $\delta = \Delta/d$ is assumed to be small, say $\delta < 0.15$. The main outcome of our theory is the prediction of a higher-order glass-transition singularity at a critical packing fraction φ^* somewhat above the critical point φ_c of the hard-sphere system and a critical width δ^* of about 0.04. This singularity organizes a subtle phase diagram and opens up various possibilities for glassy relaxation. The new results reflect the interplay of two mechanisms for particle localization, i.e. for the arrest of density fluctuations. It can either be dominated by repulsion of the particle by its cage-forming neighbors, or by the formation of bonds to the boundaries of the cage. Preliminary calculations [24,25] based upon Baxter's adhesive-hard-sphere model [27] hinted at some findings to be derived in this paper. Baxter's model treats the limit $\delta \rightarrow 0$, so it cannot deal with the indicated singularity at δ^* . Moreover, taken literally, the Baxter model cannot be used as a basis of MCT applications, since there appears a divergency due to excitations with large wave vectors. The results for this model in Refs. [24–26] depend in an ill-defined manner on the large- q cutoff used there, a problem which is avoided with the SWS.

Dense systems of colloidal particles characterized by a hard core and strong attractions of a range smaller than the core diameter by a factor of at least 10 were realized experimentally, when adding nonadsorbing polymers to either a suspension of colloidal hard spheres [28] or to emulsions [30], in solutions of sterically stabilized particles when decreasing the solvent quality [31–34], and in copolymer micellar systems when changing the temperature [35]. Such systems were also studied in Monte Carlo simulations [36,37]. Non-equilibrium phenomena characterized by a number of aspects were found which cannot be understood from the glassy states formed in hard-sphere solutions. First, amorphous solids could be formed by increasing the attraction strength even though the packing fraction was kept fixed well below the value of the hard sphere glass transition [30–34]. Second, increasing the strength of a short-ranged attraction by adding small polymers, melting of the glass states was reported for the colloid-polymer mixtures [29,28]. Third, the non-decaying frozen structures seen when immersing polymer coated colloidal particles into solvents of decreasing quality [32] exhibited a much larger Debye-Waller factor at small wave vectors than hard-sphere systems. This indicates a much higher rigidity of the solid states on intermediate length scales. In support of this observation, viscoelastic measurements for intermediate frequencies found strongly concentration dependent elastic moduli [30,31,33,34]. It will be shown that our results provide a qualitative explanation of the reported findings.

The paper is organized as follows. In Sec. II, we report our results for the structure factor of the SWS and discuss those features which cause various qualitative results of the MCT solutions. Section III presents the main result of this paper, showing the phase diagram, and discussing the properties of the glass states resulting from the interplay between attraction and repulsion. In Sec. IV, we present some results for the dynamics which illustrate that the higher order glass-transition singularities cause relaxation stretching which is much more pronounced than is known for the HSS. The last Sec.V presents some concluding remarks.

II. STRUCTURE FACTOR CALCULATIONS

A. The Model

The structure factor S_q is the essential input information needed to formulate the MCT equations. In this section, S_q shall be discussed for the square-well system (SWS). Only such states shall be considered for which S_q depends smoothly on the particle density ρ , on the temperature T , and on the wave number q . The interaction potential $V(r)$ for particles with separation distance r consists of a hard-core repulsion for $r < d$, and it has the negative value $-u_0$ within the attraction shell $d < r < d + \Delta$. The structure can be specified by three control parameters: the packing fraction φ of the hard cores, the ratio θ of thermal and attractive energy, and the relative width δ of the attraction shell:

$$\varphi = \pi\rho d^3/6, \quad \theta = k_B T/u_0, \quad \delta = \Delta/d. \quad (1)$$

Let us note the standard concepts needed for a discussion of S_q [4]. $g(r)$ and $h(r) = g(r) - 1$ abbreviate the pair distribution and the total correlation function, respectively. The Fourier transform h_q of the latter determines the structure factor $S_q = 1 + \rho h_q$. The Ornstein-Zernike equation formulates an integral equation for $h(r)$, where the kernel is the direct correlation function $c(r)$. In the wave vector domain, it reads $S_q = 1/[1 - \rho c_q]$, where

$$c_q = \frac{4\pi}{q} \int_0^\infty dr \sin(qr)[rc(r)]. \quad (2)$$

Baxter's method of the Wiener-Hopf factorization [4,38] shall be used to reformulate the Ornstein-Zernike equation. The basic concept of this theory is the factor function $Q(r)$. It is defined as a continuous real function for $r \geq 0$, determining S_q via its Fourier transform:

$$S_q^{-1} = \hat{Q}(q)\hat{Q}(q)^*, \quad (3a)$$

$$\hat{Q}(q) = 1 - 2\pi\rho \int_0^\infty dr \exp(iqr)Q(r). \quad (3b)$$

It is anticipated that $Q(r)$ as well as $c(r)$ vanishes beyond a certain distance R . For $0 \leq r \leq R$, there holds

$$rc(r) = -Q'(r) + 2\pi\rho \int_r^R ds Q'(s)Q(s-r). \quad (4)$$

Furthermore, one finds for $r > 0$

$$rh(r) = -Q'(r) + 2\pi\rho \int_0^R ds (r-s)h(|r-s|)Q(s). \quad (5)$$

For the SWS, $g(r) = 0$ is fulfilled for $0 < r < d$, and therefore, using $h(r) = g(r) - 1$, Eq. (5) splits into three subequations. Most simple is the result for the middle part, $\Delta \leq r \leq d$, where the formula known from the theory for the hard-sphere system (HSS) is reproduced:

$$Q'(r) = ar + b. \quad (6a)$$

Here, coefficients a and b are introduced by

$$a = 1 - 2\pi\rho \int_0^{d+\Delta} ds Q(s), \quad b = 2\pi\rho \int_0^{d+\Delta} ds s Q(s). \quad (6b)$$

Writing $G(r) = rg(r)$, one finds for small distances, $0 \leq r \leq \Delta$,

$$Q'(r) = ar + b - 2\pi\rho \int_{r+d}^{d+\Delta} ds G(s-r)Q(s), \quad (6c)$$

and for the attraction shell, $d \leq r \leq d + \Delta$, one obtains

$$Q'(r) = ar + b - G(r) + 2\pi\rho \int_0^{r-d} ds G(r-s)Q(s). \quad (6d)$$

Some approximation for $c(r)$ has to be introduced into Eq. (4) in order to close the system of Eqs. (4) and (6). In this paper, the Percus-Yevick approximation (PYA) and the mean-spherical approximation (MSA) shall be applied [4]. Nezbeda already studied the structure factor for the SWS using the PYA for small well widths [39,40]. His equations could be solved only in a restricted region of parameters. Since the boundary of this region of applicability is close to the parameter region $\varphi \approx 0.5$, $\theta \approx 1$ of interest in this paper, it does not seem appropriate to base the following calculations on these results.

B. Approximations

Within the PYA, one writes $c(r) = g(r)[1 - \exp(V(r)/k_B T)]$ outside the hard core. Substitution of this ansatz into Eq. (4) and using Eq. (6d) leads to the approximation for $d \leq r \leq d + \Delta$

$$e^{-u_0/k_B T} G(r) = ar + b - 2\pi\rho \int_r^{d+\Delta} ds Q'(s)Q(s-r) + 2\pi\rho \int_0^{r-d} ds G(r-s)Q(s). \quad (7)$$

Equations (6) and (7) for $Q(r)$ and $G(r)$ are solved numerically. To proceed, the equations are discretized straightforwardly. On each of the three r -intervals, a grid of equally spaced points r_n is chosen, where $n = 1, 2, \dots, 1000$. The functions $Q'(r)$ and $G(r)$ are calculated iterating Eqs. (6) and (7). At each step, the function $Q(r)$ is evaluated from $Q'(r)$ using a 5-point numerical integration. The procedure is carried out until the difference between two successive iterations summed over all points of the r -grid becomes less than 10^{-12} . The integral in Eq. (3b) is determined by a simplified Filon procedure to obtain $\hat{Q}(q)$ and hence S_q .

The MSA uses $c(r) = -V(r)/k_B T$ outside the hard core. Substituting this ansatz into Eq. (4), after integration one obtains for $d \leq r \leq d + \Delta$

$$Q(r) = 2\pi\rho \int_r^{d+\Delta} ds Q(s)Q(s-r) + [(d+\Delta)^2 - r^2] / (2\theta). \quad (8)$$

Equations (6) and (8) are solved analytically in a leading and next-to-leading order expansion, using the well width δ as the small parameter. For the organization of the expansion, the quantity $K = \delta/\theta$ is considered fixed. This procedure is motivated by Baxter's theory of sticky hard spheres [27]. He evaluated S_q in the limit $\delta \rightarrow 0$, $u_0 \rightarrow \infty$, keeping a parameter equivalent to K fixed. Details of the calculation can be found in the appendix. The hard core diameter d shall be used as the unit of length. For $\delta \leq r \leq 1$, the factor function is the parabola known from the theory of the HSS:

$$Q(r) = ar^2/2 + br + c, \quad (9a)$$

with a , b , and c now being smooth functions of the SWS control parameters. For $0 \leq r \leq \delta$, there is an enhancement above this parabola:

$$Q(r) = ar^2/2 + br + c + 2\varphi K^2 \cdot \delta [1 - (r/\delta)]^3. \quad (9b)$$

Within the attraction shell, the leading order result describes a linear decrease of $Q(r)$ from K to zero. The leading correction adds a quadratic modification. One finds for $1 \leq r \leq 1 + \delta$

$$Q(r) = K \left[1 - \frac{r-1}{\delta} \right] + K\delta \cdot \left\{ \frac{1}{2} \left[1 - \left(\frac{r-1}{\delta} \right)^2 \right] + 6\varphi c_0 \left[1 - \frac{r-1}{\delta} \right]^2 \right\}. \quad (9c)$$

Here and in the following we denote the constants from Eq. (9) as $a = a_0 + K\delta \cdot a_1$, $b = b_0 + K\delta \cdot b_1$, and $c = c_0 + K\delta \cdot c_1$. The leading order contributions are the result of the Baxter limit $\delta \rightarrow 0$:

$$a_0 = \left[\frac{1 + 2\varphi}{(1 - \varphi)^2} \right] - \frac{12K\varphi}{(1 - \varphi)}, \quad (10a)$$

$$b_0 = \left[\frac{-3\varphi}{2(1-\varphi)^2} \right] + \frac{6K\varphi}{(1-\varphi)}, \quad (10b)$$

$$c_0 = \left[\frac{-1}{2(1-\varphi)} \right] + K. \quad (10c)$$

The terms in brackets exhibit the results for the HSS [4]. The coefficients of the next-to-leading-order contributions are

$$a_1 = [6\varphi(5\varphi - 2) - 72c_0\varphi^2(1 - \varphi)] / (1 - \varphi)^2, \quad (11a)$$

$$b_1 = [9\varphi(1 - 2\varphi) + 36c_0\varphi^2(1 - \varphi)] / (1 - \varphi)^2, \quad (11b)$$

$$c_1 = [1 - 7\varphi + 12c_0\varphi(1 - \varphi)] / (2(1 - \varphi)). \quad (11c)$$

Substitution of Eq. (9) into Eq. (3b) yields $\hat{Q}(q)$ as a combination of trigonometric functions. It is elementary to work out the somewhat lengthy expression and thus via Eq. (3a) the desired result for S_q .

The large- q asymptote of the direct correlation function c_q shall be obtained from Eq. (2) by evaluating the asymptote of the Fourier-sine transform of the function $f(r) = rc(r)$. From Eq. (4) one concludes, that $f(r)$ is smooth except for at most three points $r^{(1)} = \delta$, $r^{(2)} = 1$, and $r^{(3)} = 1 + \delta$. At these points there can be a discontinuity, given by that of the derivative of the factor function: $f^{(i)} = Q'(r^{(i)} - 0) - Q'(r^{(i)} + 0)$. Let us also note from Eq. (4) the initial value $f(r = 0) = A = -Q'(0) - 6\varphi Q(0)^2$. For the exact solution of the problem, $A = 0$ must hold, but due to the approximation scheme used here, a finite value of $\mathcal{O}(\delta)$ remains: $A = -K\delta [12\varphi c_0(c_1 + 2K\varphi) + b_1] + \mathcal{O}(\delta^2)$. Thereby, the Baxter result [27], $A = \mathcal{O}(\delta^0)$, is improved. The $f^{(i)}$ can be determined easily from Eq. (9), in particular $f^{(1)} = 0$. Integrating by parts, the integral in Eq. (2) becomes: $[f^{(0)} + \sum_i f^{(i)} \cos(qr^{(i)})] / q + \mathcal{O}(1/q^2)$. Hence one arrives at $c_q = c_q^{\text{as}} + \mathcal{O}(1/q^3)$, where the asymptotic tail reads

$$c_q^{\text{as}} = (4\pi/q^2) \cdot [A + B \cos(q) + 2C \sin(q(1 + \delta/2)) \sin(q\delta/2)]. \quad (12)$$

The second term in the bracket has a form familiar from the PYA result for the HSS. But the coefficient B is a smooth function of K and δ which reduces to the HSS value for $K = \delta = 0$:

$$B = a + b + K(12\varphi c_0 - 1). \quad (13a)$$

The third term in the bracket is due to the existence of the attraction well. Its prefactor reads

$$C = (1 + \delta)/\theta. \quad (13b)$$

C. Results

The spinodal lines of the SWS are shown in Fig. 1 for three representative values of the well width δ . They

specify the divergence points of the compressibility, i.e. the zeros of S_q^{-1} for $q = 0$. The spinodal is the boundary of the regime of absolute instability with respect to the liquid-vapor transition. Only states outside this regime can be considered in the following. Substitution of Eq. (9) into Eq. (3b) yields elementary expressions for $\hat{Q}(0)$ within MSA. We have not been able to determine the spinodals within the PYA, due to numerical instability of the algorithm. The high-density regime investigated in the following applications of the MCT is indicated as the strip between the two dotted vertical lines.

Figure 2 exhibits structure factors S_q calculated within the MSA for $\delta = 0.05$, and the corresponding pair distributions $g(r)$, calculated numerically from Eq. (5), for states marked by diamonds in Fig. 1. The S_q -versus- q curves exhibit a principal refraction peak as known from other simple liquids [4]. It is caused by the hard-core driven excluded volume phenomenon, $g(r < d) = 0$. The high-temperature curves 1 and 2 exhibit peaks, which are only slightly smaller and somewhat broader than the peaks of a HSS at the same densities. The attraction modifies the pair correlations and thus the excluded volume effects, as can be inferred by comparing the curves 1 and 3. Lowering T , the short-ranged attraction causes the particles to move closer, i.e. the most probable interparticle spacing decreases. Therefore, the peak position shifts to higher q upon cooling. The distribution $g(r)$ develops a more rapidly varying structure at distances which are multiples of the particle diameter, and this explains the decrease of the peak height and the increase of the peak wings in S_q . A change of the density at low temperature modifies the peak in a similar manner as discussed above for large T , cf. curves 3 and 4. However, lowering φ drives the system closer to the spinodal, and therefore the exhibited change of S_q for small q is larger than expected for a HSS.

Results for the pair correlation $g(r)$ obtained by different closures of Eqs. (4) and (5) and by other methods have been published by Lang *et al.* [37]. For both a small and a large well width considered there, $\delta = 0.03$ and $\delta = 0.5$ respectively, we find our results for $g(r)$ in agreement with the Monte-Carlo simulation results obtained by Lang *et al.* Only for the small well width, $g(r)$ is underestimated in the well regime, $1 < r < 1 + \delta$, by about the same amount as Nezbeda's approximation [39,40] overestimates $g(r)$. At $r > 1 + \delta$, however, our solution appears to be in better agreement with the simulation results. This behaviour is similar to what holds for the optimized random-phase approximation [37].

The large- q tail of c_q will be of importance in the following. In Fig. 3 it is shown that the asymptote, Eq. (12), describes c_q very well for $q > 20$. The results have been evaluated for the state discussed in Fig. 2 with the label 3, where $(A, B, C) = (-0.092, 1.63, 7)$. The tail consists of a part due to the first two terms in Eq. (12), which differs from the HSS result merely by modifications of

the coefficients A and B . This part of the asymptote is shown in Fig. 3 (dotted line) in order to emphasize that the last contribution in Eq. (12) can be dominant. The next-to-leading order contributions to our results are not relevant for a discussion of the qualitative features of the tail. Therefore, let us write the lowest order formula for the tail as $c_q^{\text{as}} = c_q^{\text{rep}} + c_q^{\text{att}}$. Here, the coefficients of c_q^{rep} are obtained via a Baxter-like limit, $\delta \rightarrow 0$, $K = \delta/\theta$ fixed. Noting $A \rightarrow 0$ in this limit, we find

$$c_q^{\text{rep}} = (4\pi/q^2)B_0 \cos(q). \quad (14a)$$

The attraction-induced tail in this approximation reads

$$c_q^{\text{att}} = (4\pi/q^2) \cdot K(2/\delta) \sin(q\delta/2) \sin(q(1 + \delta/2)). \quad (14b)$$

For the example in Fig. 3, $(B_0, K) = (4/3, 1/3)$. For q below an upper cutoff $q_u = \pi/\delta$, the function in the bracket of Eq. (14b) increases almost linearly with q . This explains the increasing importance of the c_q^{att} contribution relative to the c_q^{rep} one, as is demonstrated in Fig. 3. If K is sufficiently large or if $|B_0|$ is sufficiently small, one can identify a lower cutoff $q_l = |B_0|/K$ such that c_q^{att} dominates c_q^{rep} :

$$c_q^{\text{as}} = (4\pi K/q) \sin(q(1 + \delta/2)), \quad q_l \ll q \ll q_u. \quad (14c)$$

In the wave-vector interval between q_l and q_u , c_q exhibits a power-law decrease slower than the one of the true large- q tail, which dominates only for $q \gg q_u$.

The PYA and the MSA differ solely by their ansatz for the direct correlation function $c(r)$ within the attraction shell $1 < r < 1 + \delta$. Within the PYA, $c(r)$ depends on r via the r -dependence of the pair distribution function, $c_{\text{PYA}}(r) = [1 - \exp(-u_0/(k_B T))]g(r)$, while the MSA assumes a constant $c_{\text{MSA}} = u_0/(k_B T)$. In this paper, systems with narrow attraction shells are of interest, $\delta \ll 1$. Therefore it is a reasonable approximation to ignore the r -dependence of c_{PYA} by writing $g(r) \approx g_d = g(r = 1)$. Thus, for every state where a solution of the PYA exists, there is a solution of the MSA, yielding the same structure factor. However, the corresponding solution for the MSA has to be evaluated for an effective reduced temperature $\theta_{\text{eff}}^{\text{MSA}}$. The latter is a smooth function of $\theta = u_0/k_B T$, φ and δ , estimated by

$$\frac{1}{\theta_{\text{eff}}^{\text{MSA}}} \approx \left[1 - \exp\left(\frac{-u_0}{k_B T}\right) \right] g_d. \quad (15)$$

Consequently, the PYA and the MSA yield the same scenarios for the structure factor in the parameter regime of interest in this paper. This finding is demonstrated in Fig. 4 for the basic quantity of the structure factor theory, the factor function $Q(r)$. The result calculated within the PYA for the parameter triple

$$\varphi_{\text{PYA}}^* = 0.5293, \quad \theta_{\text{PYA}}^* = 1.1000, \quad \delta_{\text{PYA}}^* = 0.0429 \quad (16a)$$

is very close to the one obtained within the MSA for

$$\varphi_{\text{MSA}}^* = 0.5258, \quad \theta_{\text{MSA}}^* = 0.2332, \quad \delta_{\text{MSA}}^* = 0.0465. \quad (16b)$$

It will be shown in Sec. III, that the two states specified above are of central importance. The values found for the corresponding densities φ^* and well widths δ^* are close to each other. The difference in the values for the effective attraction strength $1/\theta^*$ is well explained by Eq. (15). If one inserts $g_d^* \approx 7.5$ as obtained from the MSA, one finds $\theta_{\text{eff}}^{\text{MSA}} \approx 0.2233$.

All calculations within the MSA are based on the small- δ expansion for the factor function, say $Q^{\text{exp}}(r)$, defined by Eqs. (9) to (11). To control this result, Eq. (6) and the analog of Eq. (7) for the MSA closure have also been solved numerically to get the correct MSA factor function, say $Q^{\text{MSA}}(r)$. The difference $\delta Q(r) = Q^{\text{MSA}}(r) - Q^{\text{exp}}(r)$ is positive and about 3% (1%) for $\delta = 0.25$, (0.15) for $r \leq 0.5$; and it decreases for r increasing above 0.5.

The dotted line in Fig. 4 exhibits the parabola for $Q(r)$, Eq. (9a), for coefficients of the HSS. Introduction of the attraction smoothly renormalizes the coefficients a , b , and c , such that the parabola shifts upwards and becomes flatter. There appears a region of positive values for $Q(r)$ near the core surface $r \approx 1$. These shifts cause the smooth drifts of the Fourier transform for $\hat{Q}(q)$, which lead to the drifts of S_q discussed in connection with Fig. 2 and to the appearance of a spinodal, cf. Fig. 1. The only qualitative new feature, which is caused by the attraction well, is the almost straight decrease of $Q(r)$ within the interval $1 < r < 1 + \delta$. Equation (9c) yields the slope in leading order as $Q'(r) = -K/\delta$. In the Baxter limit, this slope diverges. The specified almost constant part of $Q'(r)$ causes the attraction-tail contribution to the asymptote of c_q , Eq. (14b). The power law tail, Eq. (14c), is a precursor of the mentioned divergency.

The structure factor or the pair correlation function determine the positions of the liquid-gas transition points. However, one faces the known consistency problem that different routes for the equation of state yield different results for the transition points if approximations for S_q or $g(r)$ are used [4]. We will not discuss these problems in this paper, since it is irrelevant for the evolution of glassy dynamics or the glass transition whether the fluid is in a stable or metastable thermodynamic state.

III. THE PHASE DIAGRAM

A. The bifurcation equation

The MCT equations of motion for various dynamical quantities are based on the equations for the normalized density correlators $\phi_q(t) = \langle \rho_q^*(t) \rho_q \rangle / \langle |\rho_q|^2 \rangle$. For the liquid state these functions approach zero for large time t ; density fluctuations which were created at time $t = 0$ disappear for $t \rightarrow \infty$. The glass state is characterized by

a spontaneous arrest of these fluctuations, i.e. the long-time limits f_q of the correlators do not vanish. The ideal liquid-glass transition of the MCT is characterized by a discontinuous increase of f_q from its value zero in the liquid state to the critical Debye-Waller factor $f_q^c > 0$ of the glass. For colloidal suspensions, f_q can be deduced from the dynamical-light-scattering results for $\phi_q(t)$. The experimental findings for the HSS [10] and for a charge stabilized system [23] confirmed the discontinuity for f_q and the data for f_q^c agree well with the MCT results.

The f_q obey the equation $f_q/(1-f_q) = \mathcal{F}_q(f)$ [14]. Here, the mode-coupling functional \mathcal{F}_q is given by

$$\mathcal{F}_q(f) = \frac{1}{2} \int \frac{d^3k}{(2\pi)^3} V_{\vec{q},\vec{k}} f_k f_{|\vec{q}-\vec{k}|}. \quad (17a)$$

The mode-coupling vertices are determined by the structure factor S_q , the direct correlation function c_q , and the density ρ

$$V_{\vec{q},\vec{k}} \equiv S_q S_k S_{|\vec{q}-\vec{k}|} \rho \left[\vec{q} \cdot \vec{k} c_k + \vec{q} \cdot (\vec{q} - \vec{k}) c_{|\vec{q}-\vec{k}|} \right]^2 / q^4. \quad (17b)$$

In the following, the wave-vector integrals will be discretized to points on a grid of M values, which are equally spaced with step size h , starting at $q_{\min} = h/2$. Thereby the mode-coupling functional is changed to a second order polynomial

$$\mathcal{F}_q(f) = \sum_{kp} V_{q,kp} f_k f_p. \quad (18)$$

The explicit representation of the coefficients can be found in Ref. [41]. The M parameters f_q obey the algebraic equations

$$f_q/(1-f_q) = \mathcal{F}_q(f), \quad q = 1, \dots, M. \quad (19)$$

Besides the long-time limit f_q , Eq. (19) can have further solutions, say \tilde{f}_q , obeying $0 \leq \tilde{f}_q < 1$. The Debye-Waller factor is distinguished by the maximum property $f_q \geq \tilde{f}_q$, $q = 1, \dots, M$ [42]. We used the iteration procedure $f_q^{(n+1)} = \mathcal{F}_q[f^{(n)}]/(1 + \mathcal{F}_q[f^{(n)}])$, $n = 0, 1, \dots$ to determine f_q . With increasing n the $f_q^{(n)}$ decrease monotonically towards f_q , if the iteration is started with $f_q^{(0)} = 1$ [43].

Two concepts are needed in the following, namely the maximum eigenvalue E and the exponent parameter λ [42]. For the discussion of the implicit equations, Eq. (19), the Jacobian J is of importance. It is equivalent to $1 - C$, where the $M \times M$ matrix C is determined by

$$C_{qk} = \frac{\partial \mathcal{F}_q(f)}{\partial f_k} (1 - f_k)^2. \quad (20a)$$

Also the variation of C with changes of f is needed

$$C_{q,kp} = \frac{1}{2} \frac{\partial^2 \mathcal{F}_q(f)}{\partial f_k \partial f_p} (1 - f_k)^2 (1 - f_p)^2. \quad (20b)$$

There is a nondegenerate eigenvalue E of matrix C with the property, that all other eigenvalues \tilde{E} obey $\tilde{E} < E$. There holds $E \leq 1$, and liquid-glass transition points are determined by the condition $E = E_c = 1$. It is helpful to follow the drift of E with changes of control parameters while searching for the transition points. The left and right eigenvectors of C for the eigenvalue E , denoted by \hat{e} and e respectively, are uniquely determined by the conditions: $\hat{e}_q \geq 0$, $e_q \geq 0$, $\sum_q \hat{e}_q e_q = 1$, $\sum_q \hat{e}_q (1 - f_q) e_q^2 = 1$. They are used to characterize every transition point by a single number λ , defined as

$$\lambda = \sum_{qkp} \hat{e}_q^c C_{q,kp}^c e_k^c e_p^c. \quad (21)$$

The solutions of Eq. (19), considered as functions of the M^3 coefficients $V_{q,kp}$, can exhibit singularities, which are called bifurcation points [44]. The singularities occur if the Jacobian J is a singular matrix, i.e. if the matrix C has eigenvalue unity. The special singularities, which are exhibited by the Debye-Waller factors, are called glass-transition singularities. These are members of the simplest family of singularities, labeled A_l , $l = 2, 3, \dots$ [44]. They are topologically equivalent to the bifurcation singularities of the real roots of real polynomials of degree l . Since the $V_{q,kp}$ are smooth functions of the control parameters, in the SWS the Debye-Waller factor f_q exhibits A_l singularities considered as a function of the variables φ , θ , and δ . The liquid-glass transition is an example for the simplest bifurcation singularity A_2 , called a fold bifurcation. Such transitions occur on smooth surfaces in the 3-dimensional parameter space. These surfaces can terminate in smooth lines of A_3 singularities, that are also called cusp bifurcations. The inner points of the A_2 -surfaces are characterized by $0 < \lambda < 1$, and for the endpoints there holds $\lambda = 1$. The most complicated generic singularity in a three-parameter system is the meeting of two A_3 lines in an A_4 point. Its position shall be denoted by φ^* , θ^* , and δ^* . This singularity is also called a swallow-tail bifurcation [44]. The possibility of the described scenarios has been demonstrated earlier for schematic MCT models, invented with the mere intention of demonstrating the existence of A_3 and A_4 points [42]. This paper is the first demonstration of the existence of an A_4 for a microscopic model; the values for the SWS are given in Eq. (16).

The numerical work is done with step size $hd = 0.4$. It was checked for representative cases, that choosing smaller step sizes does not alter the results to be presented. Choosing M is equivalent to introducing an upper wave-vector cutoff $q^* = (M - 1/2)h$ in Eq. (17a). The previous comprehensive studies for the HSS [41,45] were done with $M = 100$. For sufficiently large $1/\theta$ and sufficiently small δ , the direct correlation function c_q develops a large- q tail, discussed in Eq. (14). This is decisive for

fixing the value q^* needed to ensure the correct handling of Eq. (17). If the coefficient K in Eq. (14c) is kept fixed, the cutoff q^* will increase with decreasing well-width parameter proportional to $1/\delta$. The maximum value for M that can be handled in the numerical work, defines the lower limit for $1/K$ and δ , which can be treated. We used values for M up to 2000 occasionally, in order to guarantee the cutoff independence of the results reported in this paper.

B. Results

The phase diagram for the SWS is shown in Fig. 5 for several constant- δ cuts through the three dimensional control-parameter space. The results based on the PYA and the MSA are qualitatively the same. Let us first consider the three states 1, 2, and 3 from Fig. 1 for $\delta = 0.06$. Within the MSA, state 1 refers to the liquid phase, cf. Fig. 5b. Increasing φ to the state 2 increases the height of the first sharp diffraction peak of S_q , located near $q_0 = 7$, cf. Fig. 2. Thus the compressibility for fluctuations in the shell $q \approx q_0$ increases. This leads to arrest in a glass state, as known from the HSS. If one cools state 1 at fixed $\varphi = 0.50$ down to state 3, S_{q_0} decreases, as was explained in connection with Fig. 2. This effect stabilizes the liquid, but it is overcompensated by the increase of S_q in the small-wave-vector region, $q < 6.1$, and, more important, in the large- q region, $q > 7.4$. As a result of this compressibility increase on the wings of the structure factor peak, the liquid freezes to a glass upon cooling, cf. Fig. 5. For large temperature, S_q depends only weakly on T ; the terms proportional to $K = \delta \cdot u_0/(k_B T)$ in Eqs. (9) to (11) cause only small modifications of the coefficients determining the factor function $Q(r)$. This explains, why the transition lines are almost vertical in Fig. 5a for $k_B T/u_0 > 3$ and in Fig. 5b for $\theta > 1$. The peak wings are not very sensitive to density changes by a few percent for $\varphi < 0.51$. This explains, why the transition lines in Fig. 5 are rather flat there. The two pieces of the transition line join smoothly and λ remains below unity for $\delta = 0.06$, as is shown in Fig. 6b. Thus, the described curve represents a cut through a smooth surface of A_2 bifurcations.

The mentioned high-temperature pieces of the transition surface are located at packing fractions φ_c , which exceed the value for the HSS, $\varphi_c^{\text{HSS}} \approx 0.516$. This means, that the attraction forces have stabilized the liquid phase. This effect is smaller for larger T and therefore the φ_c -versus- T_c curve decreases. There is the possibility of glass melting due to cooling, if the decrease of S_{q_0} is not overcompensated by the increase of the structure-factor-peak wings. The attraction causes bonding, in the sense that the average separation of two particles is smaller than expected for a HSS. Therefore the average size of the holes increases and this favors the long-distance motion characteristic for a liquid. Consider states with $\varphi = 0.52$ and

$\delta = 0.06$. For the MSA results one notices from Fig. 5b, that the system is in a glass for $\theta = 0.10$ and it melts upon heating if θ approaches $\theta_m^- \approx 0.30$. This transition occurs due to the temperature drift of the coupling to modes with wave vectors in the wings of the S_q peak. The system remains in the liquid upon further heating until it reenters the glass at $\theta_m^+ \approx 1.41$. This freezing is caused by the drift of the coupling to modes with $q \approx q_0$. The described reentry phenomenon [24,25] is a manifestation of two mechanisms for localization due to the cage effect in the high density SWS to be explained below.

The preceding two paragraphs can be summarized as follows. There is a subtle interplay of excluded-volume and bonding effects which determine the variations of the pair correlation function $g(r)$ on the length scale of the particle diameter d . This is reflected in the properties of the structure factor S_q for wave numbers q at and around the peak position q_0 ; the relevant q range is the one exhibited in Fig. 2. Fluctuations with longer wave length are of no qualitative importance for those parameter points studied in this paper. This conclusion was corroborated by dropping all contributions to the mode-coupling functional, Eq. (18), where k or p are smaller than 4; there was no significant change of the phase diagram calculated with the MSA structure compared to what is shown in Fig. 5b. Similarly, a cutoff $q_+ = 20$ was introduced such that all contributions to the mode-coupling functional with $q > q_+$ are dropped. The MSA results shown in Fig. 5b for $\delta = 0.09$ and $\delta = 0.06$ did not change, nor was there a noticeable change for the other curves for $\theta > 0.6$. We conclude, that the two specified sources for correlations on intermediate length scale explain the phase transition points, which are marked by open symbols in Fig. 5a or by the corresponding light lines in Fig. 5b.

To substantiate the previous conclusion, we have constructed a further phase diagram based on the MSA structure factor, using the above specified cutoff q_+ . As mentioned, the curves for $\delta = 0.09$ and $\delta = 0.06$ were reproduced up to minor deviations. Upon decreasing δ further, curves emerge, which continue the trend of the two ones for larger δ . The limit $\delta \rightarrow 0$ can be carried out; no new features appear. This ad-hoc MCT model yields a smooth liquid-glass transition surface of A_2 -bifurcation points with $\lambda < 1$. Obviously, the true phase diagram of the SWS shown in Fig. 5 is quite different. There are the transition points marked by filled symbols in Fig. 5a or by the corresponding heavy lines in Fig. 5b. These define transition lines, which do not join smoothly the previously discussed lines. Rather they cross the former lines. Thus, for sufficiently small δ and sufficiently large attraction strength $u_0/(k_B T)$, there is a new glass formation mechanism, dominated by density fluctuations with large wave number $q \geq q_+$. These are due to spatial correlations on the length scale of the attraction-well width Δ .

For a discussion of the identified new pieces of the transition surface, the mode-coupling coefficients in

Eqs. (17a) and (17b) can be simplified. As explained in connection with Fig. 3, one can write for $k = |\vec{k}| \geq q_+$ and $p = |\vec{q} - \vec{k}| \geq q_+$ the leading asymptotic expression for the structure factors, $S_k = S_q = 1$, and for the direct correlations function $c_q = c_q^{\text{as}}$, Eq. (14b). Thus, the dominant part of the mode-coupling functional depends explicitly on the control parameters by the prefactor $\varrho K^2 = \varrho (\delta u_0 / (k_B T))^2$ and otherwise only on δ via the large-wave-vector cutoff q_u . A further density dependence is due to fluctuations with $q < q_+$ only. This explains why the low- T -transition lines in Fig. 5 are so flat. K^2 decreases proportional to δ^2 , and this effect is not overcompensated by the increase of q_u . As a result, the horizontal transition lines decrease with decreasing δ . For low packing fractions, such a trend can be shown explicitly by an analytic calculation [25,46]. Along this transition line, λ increases with increasing φ until it approaches unity signaling an endpoint at some $\varphi_c^\circ(\delta)$, $\theta_c^\circ(\delta)$. This is demonstrated in Fig. 6a for three values of δ and in Fig. 6b for $\delta = 0.03$. The line stops the previously discussed line in some crossing point. Between the crossing point and the endpoint, there occur glass-glass transitions. Upon increasing δ , the length of the glass-glass transition line shrinks, until it vanishes for some δ^* at some $\varphi^* = \varphi_c^\circ(\delta^*)$ and $\theta^* = \theta_c^\circ(\delta^*)$; and this is the A_4 singularity whose coordinates are listed in Eq. (16).

Every pair of glass states can be connected by a curve in parameter space such that, upon shifting the control parameters φ , θ , and δ along this curve, the glass properties change smoothly. Thus one cannot discriminate precisely between repulsion- and attraction-dominated glass states. However, upon crossing the glass-glass-transition surface, there occurs a discontinuous change of the glass-state properties. These discontinuities can be used to differentiate quantitatively between the two types of glasses. From a mathematical point of view, the situation is analogous to the termination of the liquid-gas-transition line at the critical point. Some results shall be presented from the theory based on the PYA for S_q . Let us consider states for $\varphi \approx 0.54$ for the smallest δ used in Fig. 5a. Figure 7 exhibits as filled symbols the decrease of the Debye-Waller factor for three representative wave numbers, if the attraction-dominated glass is heated towards the transition temperature T_c , $k_B T_c / u_0 = 1.0471 = \theta_c$. The f_q decrease towards the critical value f_q^c according to the asymptotic square root law $f_q - f_q^c \propto h_q \sqrt{\theta_c - \theta}$, which is the signature of the fold bifurcation [42]. Upon crossing the line into the repulsion-dominated glass, f_q drops and keeps on decreasing upon further heating up to $\theta \approx 1.3$, as shown by the open symbols. Notice, that f_q does not exhibit any singularity for θ decreasing towards θ_c . The remarkable variation of f_q for θ near but above θ_c is a precursor phenomenon of the nearby A_3 singularity. The f_q for $\theta > \theta_c$ is smaller than the Debye-Waller factor for the HSS at the same packing fraction. Hence the attraction has softened the glass. This effect has to

disappear for very large T , and this explains, why f_q increases again, reflecting a glass stiffening upon heating. The described effects for $\theta > \theta_c$ are the counterparts to what was discussed above in connection with the reentry phenomenon.

The wave-vector dependence of f_q changes qualitatively upon crossing the glass-glass-transition line as is shown in Fig. 8. Let us focus in this paragraph on the wave-vector regime at and above the structure factor peak position $q \gtrsim q_0 \approx 7$. Here, f_q oscillates with wave-vector scale $2\pi/d$ around the Mößbauer-Lamb factor f_q^s . The latter is the analog to f_q , constructed for a tagged particle with position vector $\vec{r}_s(t)$ via its density-correlator $\phi_q^s(t) = \langle \rho_q^s(t) \rho_q^s(0) \rangle$; $\rho_q^s(t) = \exp(i\vec{q}\vec{r}_s(t))$. This quantity, in particular its long-time limit f_q^s , can also be measured [13]. One finds $f_q^s = 1 - q^2 r_l^2 + \mathcal{O}(q^4)$, where r_l is the localization length of the particle: $r_l^2 = \lim_{t \rightarrow \infty} \langle |\vec{r}_s(t) - \vec{r}_s(0)|^2 \rangle$ [42]. In the Gaussian approximation, one can write $f_q^s = \exp(-q^2 r_l^2)$ so that the half-width-wave vector q_l , defined by $f_{q_l} = 0.5$, can be used to estimate $r_l \approx 1/q_l$. For the Debye-Waller factors on the high-temperature side of the transition line, which are shown as full lines in Fig. 8, one estimates $q_l \approx 20$. The localization length $r_l = 0.05$ is about the same size as expected for a particle rattling between the hard walls of its cage in a HSS. The f_q and r_l are close to those of a HSS [42,45]. However, on the low-temperature side of the transition, the f_q vary by less than 10% if q increases up to $2q_0$, as shown by the dashed lines in Fig. 8. The wave number q_l is much larger than expected from the free volume in the cage. At the transition, $q_l \approx 44$, i.e. the localization length is decreased discontinuously by a factor of about 2.3. For $\theta = 0.9$ and 0.6 the localization length is about 0.01 and 0.006 , respectively. This shows that the localization length is of order δ . The particle is bound to the wall of the cage and localization is determined entirely by the particle attraction. This localization mechanism via bond formation is operative at low packing fractions also, and it has been studied within MCT in this regime. There, bond formation has been argued to be of importance for colloidal gelation [25,46,47].

There is no strong dependence of f_q on wave numbers $q < 4$. The low-temperature glass is distinguished from the high-temperature one by the fact that the zero-wave-number limit of the Debye-Waller factor, f_0 , is larger for the former than for the latter. Therefore, upon crossing the glass-glass-transition surface by cooling, the peak for $q \approx q_0$ of the f_q -versus- q diagram disappears, Fig. 8. The number f_0 is related to the longitudinal elastic modulus of the system. This consists of a part expected for the ergodic liquid and a part m_0 reflecting the incomplete relaxation of the non-ergodic glass [42]. The latter is given by the zero-wave-number limit of the mode-coupling functional, Eq. (18), $m_0 = \mathcal{F}_0(f)$. The $q = 0$ limit can be carried out easily in Eq. (17b), so that one derives from Eq. (17a) a formula [14],

$$m_0 = \int_0^\infty dk v^L(k) f_k^2. \quad (22)$$

After discretization, one can substitute the results for f_k to get m_0 , and via Eq. (19) one has $f_0 = m_0/(1+m_0)$. For the glass with $\theta > \theta_c$, the integral in Eq. (22) is dominated by fluctuations on the intermediate wave-vector scale, $k \approx q_0$. As known from the HSS, m_0 is of order unity and thus f_0 is about 0.5. However, for $\theta \leq \theta_c$, the integral is dominated by large- k fluctuations. This enhances m_0 . For $\theta = \theta_c$, one finds $m_0 \approx 12.7$ and this increase of the modulus explains the increase of f_0 to about 0.927, exhibited by the lowest dashed line in Fig. 8. Decreasing the temperature to $k_B T/u_0 = 0.6$, leads to $m_0 \approx 385$ and this explains the large value $f_0 \approx 0.997$, exhibited by the uppermost dashed curve in Fig. 8. For the shear modulus G' , a formula like Eq. (22) holds, where the expression for v^T is similar to that for v^L [14]. Therefore, the shear modulus also exhibits the specified strong enhancement due to the attraction wells. Figure 9 shows that the dramatic change of the moduli is the most relevant feature to be observed upon crossing the glass-glass-transition surface. The strong short-ranged attraction causes bond formation, and this increases the rigidity of the glass with respect to compressions or shearing considerably relative to that of a glass at a similar density, where the structural arrest is dominated by mere hard-sphere repulsion.

IV. STRUCTURAL RELAXATION

A. Some general MCT equations

The MCT equations of motion are based on the exact expression of the density correlator $\phi_q(t)$ in terms of a fluctuating-force correlator [4,5], which in turn is split into a part treating normal liquid effects, and a relaxation kernel $m_q(t)$ describing the cage-effect contribution. This kernel is approximated by the mode-coupling functional, discussed above in connection with Eqs. (17) and (18): $m_q(t) = \mathcal{F}_q[\phi(t)]$, [14,42]. This paper will be restricted to the simplest approximation for the normal liquid effects, i.e. the colloid will be treated as a system of Brownian particles, so that only the instantaneous correlations as given by the structure factor S_q are incorporated. As a result one obtains [41]:

$$\tau_q \partial_t \phi_q(t) + \phi_q(t) + \int_0^t m_q(t-t') \partial_{t'} \phi_q(t') dt' = 0. \quad (23)$$

This equation implies the short-time asymptote $\phi_q(t) = 1 - (t/\tau_q) + \mathcal{O}(t^2)$. For the time scale, one finds $\tau_q = S_q/(D_0 q^2)$, where D_0 denotes the single-particle diffusion coefficient. D_0 reflects the property of the solvent, and it fixes the time scale for the transient motion. The unit of time shall be chosen such that $1/D_0 = 160$ to ease

comparisons with the results for the HSS from preceding work [41,45].

Two comments on the implications of Eq. (23) might be appropriate. First, the solutions are completely monotone functions, i.e. there is a rate density $\rho_q(\gamma) \geq 0$, normalized to $\int_0^\infty \rho_q(\gamma) d\gamma = 1$, such that

$$\phi_q(t) = \int_0^\infty e^{-\gamma t} \rho_q(\gamma) d\gamma. \quad (24)$$

Thus, the MCT approximations maintain a fundamental property of colloidal dynamics: auto-correlation functions can be written as superpositions of Debye-relaxation functions [43]. Second, outside the transient, the solutions can be written as $\phi_q(t) = F_q(t/t_0)$. Here, F_q is given by the mode-coupling functional \mathcal{F}_q , i.e. by the equilibrium structure factor S_q . The transient dynamics, no matter how complicated, enters via the single time scale t_0 only [16,48,49]. The following results for the long-time dynamics are thus not influenced by the simplified treatment of the short-time dynamics in Eq. (23), except up to a change of the overall time scale t_0 . It is known that the short-time dynamics in colloids is influenced by hydrodynamic interactions [2]. Unfortunately, it is not known how to incorporate these interactions in a theory for high-density colloids. But we consider it plausible, that the hydrodynamic interactions merely renormalize the transient dynamics [50], thereby being irrelevant for the structural-relaxation effects.

For control parameters approaching a glass-transition singularity, there appears an increasingly larger dynamical window, where the solutions are arbitrarily close to the critical Debye-Waller factor f_q^c . Therefore, one can solve the MCT equations of motion by an asymptotic expansion, using $\delta\phi_q(t) = \phi_q(t) - f_q^c$ as a small parameter. The result can be expressed in the form

$$\phi_q(t) - f_q^c = h_q G(t) + h_q^{(1)} G^{(1)}(t) + \dots \quad (25)$$

Most of the known universal results for the MCT bifurcation dynamics are based on the understanding of the leading-order contribution $G(t)$. The next-to-leading-order term $G^{(1)}(t)$ allows to discuss the range of validity of the leading-order formulas. A comprehensive demonstration of the cited results for the HSS can be found in Refs. [41] and [45].

Equation (25) reduces to a particular transparent form for the critical dynamics, i.e. for control parameters placed on the glass-transition points. For the fold bifurcation, one finds a power-law decay:

$$G(t) = (t_0/t)^a, \quad G^{(1)}(t) = (t_0/t)^{2a}; \quad A_2. \quad (26a)$$

The critical exponent a is given by the exponent parameter λ via $\Gamma(1-a)^2/\Gamma(1-2a) = \lambda$, $0 < a \leq 0.5$. The end-points of the A_2 -bifurcation surfaces are characterized by exponent a approaching zero. For the cusp bifurcation, there holds [51]:

$$G(t) \propto 1/\ln(t/t_0)^2, \\ G^{(1)}(t) \propto \ln(\ln(t/t_0))/\ln(t/t_0)^3; \quad A_3. \quad (26b)$$

For the swallow-tail bifurcation, one has [51,52]:

$$G(t) \propto 1/\ln(t/t_0), \\ G^{(1)}(t) \propto \ln(\ln(t/t_0))/\ln(t/t_0)^2; \quad A_4. \quad (26c)$$

The dependence of the leading-order contribution $G(t)$ on the control parameters is well understood, but shall not be considered in this paper.

B. Results

Let us first estimate the dynamical window relevant for the discussion. For the HSS, the correlators $\phi_q(t)$ decay from 1.00 to 0.95 for times increasing up to about $t = 1$ for representative wave vectors. In this sense, $t = 1$ is the scale for the transient dynamics. After a crossover window of about one or two decades, the leading-order asymptotic law $\phi_q(t) = f_q^c + h_q G(t)$ becomes valid at about $t = 10^2$. This value may be an order of magnitude smaller or larger, depending on the wave number q [41]. The same is true for the data obtained by van Meegen *et al.* for hard-sphere colloids, provided one identifies the time unit $t = 1$ with 1 msec [17]. The correlators have been measured up to 10^6 msec, and thus the so far explored windows extend up to 10^6 in the units used here. This limit might shift up in future work, using different experimental setups.

Figure 10 exhibits the critical correlators $\phi_q^c(t)$ for $q = 4.2$ for five states on the transition line $\delta = 0.0465$ through the A_4 singularity. The states 1 and 5 refer to an exponent parameter $\lambda \approx 0.80$ on the side of the attraction-dominated and repulsion-dominated glass, respectively. For times of the order of 10^3 and larger, the leading-order formula, $\phi_q(t) - f_q^c \propto (t_0/t)^a$, $a \approx 0.28$, describes the results. Thus, the scenario is similar to the one known from the HSS, and this is also true for other states on the line with $\lambda < 0.80$. However, if one considers states closer to the A_4 point, the onset of the critical power law gets shifted to larger times. This is demonstrated for the two states 2 and 4, which deal with $\lambda \approx 0.90$. For the state 4, the t^{-a} law with $a \approx 0.20$ is valid only for $t > 10^6$. This trend continues, if one moves even closer to the A_4 point, whereby λ increases even further; compare Fig. 6. At the A_4 singularity, the correlator decays from 1.00 to $f_q^c \approx 0.77$. This decay is stretched so enormously, that even for $t = 10^{12}$ it only reaches the value $\phi_q(t) \approx 0.80$, as is shown by curve 3 in Fig. 10. One can describe the critical correlator with Eqs. (25) and (26c) for the window $10^{15} < t < 10^{25}$, using h_q and $h_q^{(1)}$ as fit parameters. But this fit does not describe the correlator for $t < 10^{10}$. Thus one concludes, that the critical correlator of the A_4 for the SWS cannot

be described by the asymptotic Eq. (26c) within accessible dynamical windows. Nor can the critical power-law decay of the A_2 singularity be measured, if λ exceeds a certain value, say 0.9. Thus, there is a part of the transition lines near the A_4 point, characterized by $\lambda \geq 0.9$, where the correlators exhibit structural relaxation patterns towards the plateau values f_q^c that are stretched up to $t = 10^6$ or larger. The known asymptotic formulas cannot be used to describe the MCT solutions within this regime.

The liquid dynamics on the small- δ side of the A_4 point is particularly subtle, since there is an A_3 singularity in addition to the line-crossing point. Figure 11 exhibits as an example such a situation for $\delta = 0.03$. Parameters on a straight line, $\theta = 0.1875$, which is slightly above the A_3 point, are considered. The transition to a repulsion-dominated glass state then occurs at $\varphi_c = 0.5360$. At the transition point, the critical Debye-Waller factor is $f_q^{(1)c} \approx 0.50$, and the exponent parameter is given by $\lambda = 0.847$, implying a critical exponent $a = 0.250$. Curve 3 was calculated for such small distance from the transition point, $-\varepsilon = (\varphi_c - \varphi)/\varphi_c = 7.9 \cdot 10^{-4}$, that $\phi_q(t)$ decays to zero just within the dynamical window displayed in the figure. The dash-dotted line with label A presents the leading-order critical law for the A_2 singularity, Eqs. (25) and (26a), with the time scale t_0 fitted to the decay at long times for $\varphi = \varphi_c$. One observes the same phenomenon as explained above in connection with Fig. 10: since λ is rather large, the asymptotic law describes the data only for rather large times, $t > 10^{5.5}$. After falling below the plateau value $f_q^{(1)c}$, the correlator decays towards zero. This is the α process, and it starts with the von-Schweidler asymptote $f_q^{(1)c} - h_q(t/\tau)^b$, which is shown by the dash-dotted line with label B. The exponent $b = 0.396$ obeys a similar relation as the critical exponent, $\Gamma(1+b)^2/\Gamma(1+2b) = \lambda$. Thus the structural relaxation connected with the liquid-glass transition follows the known scenario, except that the familiar A_2 patterns can be observed only for times far out the transient regime, $t > 10^{5.5}$.

Figure 11 exhibits a large dynamical window, $10^2 < t < 10^{5.5}$, where the structural relaxation does not follow the asymptotic laws for a fold bifurcation. Instead, the dashed straight line demonstrates that the correlator labeled 3 follows a logarithmic decay law,

$$\phi_q(t) = f_q^{(2)c} - C_q \ln t, \quad (27)$$

for the major part of the mentioned window, $10^2 \leq t \leq 10^{4.5}$. Here, $f_q^{(2)c} \approx 0.87$ is the Debye-Waller factor at the A_3 singularity. There is a line through every A_3 singularity, which is transversal to the transition line ending at the A_3 , such that Eq. (27) is a leading-order solution for the MCT equations of motion on a certain intermediate time window. The length of the window expands and the prefactor C_q in front of the $\ln t$ decreases, if one moves closer towards the A_3 point [53]. These results explain the appearance of the $\ln t$ part and the change of its

prefactor, if one compares curve 2 with curve 3 in Fig. 11. One concludes that it is the bifurcation dynamics of the A_3 singularity which prevents the evolution of the t^{-a} law for the fold bifurcation. Similarly, the α process for curve 2 does not start with von Schweidler's law. Therefore, contrary to what one observes for the dynamics of the HSS for comparable large times [41], the α processes for curves 2 and 3 do not obey the superposition principle. Close to the A_3 point, the dynamics outside the transient and preceding the onset of the $\ln t$ -decay law follows the critical law for the A_3 , as given by Eqs. (25) and (26b). But for the shown curves, the situation is similar as explained comprehensively for the critical decay for the HSS [41]. The plateau $f_q^{(2)c}$ is so high, that there is only a small variation remaining for the $1/(\ln t)^2$ law to manifest itself. The correction terms for the cited leading-order and next-to-leading-order contributions are so large, that one has to consider states much closer to the A_3 to see the result of Eq. (26b).

For state 1, the A_2 , A_3 , and A_4 singularities are so far away, that none of the cited asymptotic laws is clearly developed. On the other hand, they are close enough to cause a considerable relaxation stretching. The correlator $\phi_q(t)$ needs a dynamical window of three orders of magnitude to complete the 80% of its decay from 0.9 to 0.1, as is shown in Fig. 11.

In Fig. 12a, a set of correlators $\phi_q(t)$ for five representative wave numbers is shown. The state refers to the liquid close to the A_4 point. For $q = 24.2$, the window for the logarithmic decay extends from $t = 10^3$ to $t = 10^{10}$. For the other wave numbers, the corresponding windows are smaller, i.e. the window of validity for the leading-order asymptotic laws depends on the chosen correlator. If the correction term $h_q^{(1)}G^{(1)}(t)$ in Eq. (25) could be neglected, i.e. if the factorization theorem $\phi_q(t) - f_q^c = h_q G(t)$ would hold, the rescaled correlators $\hat{\phi}_q(t) = [\phi_q(t) - f_q^c] / h_q$ should collapse on the common function $G(t)$. In particular, all correlators should cross their plateau value f_q^c at the same time t_- , given by $G(t_-) = 0$. The latter property is fulfilled within a small error margin for $t_- = 8.9 \times 10^5$. Figure 12b demonstrates the validity of the factorization property for a two-decade window. The size of this window is considerably smaller than the one found for the HSS for a state with a similar overall relaxation time [41]. Thus, the next-to-leading-order correction in Eq. (25) is much larger near the A_4 than the one known from the bifurcation dynamics of the simple HSS.

V. CONCLUSIONS

In this paper, ideal liquid-glass transitions and the evolution of glassy dynamics were analyzed within the basic version of the mode-coupling theory (MCT) for a simple colloid model, where the particles interact via a square-well potential. The discussion was restricted to the high-

density regime. Hence the excluded-volume effects play a crucial role for the structure, and the cage effect is an essential feature of the dynamics. The presence of short-ranged attractions leads to a variety of new features compared to the ones known from the hard-sphere system (HSS). We find a subtle phase diagram for the glass-transition lines in the plane spanned by the two control parameters, packing fraction φ and reduced temperature θ (Fig. 5). The diagram is organized around an A_4 -glass-transition singularity. This occurs for a critical value $\delta^* \approx 0.04$ of the ratio δ of the attraction-well width and the hard-core diameter, a packing fraction φ^* exceeding the transition density φ_c^{HSS} of the HSS, and a certain critical temperature, cf. Eq. (16).

For $\delta > \delta^*$ and sufficiently low temperature, there is a part of the liquid-glass transition line, where the critical temperature θ_c increases with the critical density φ_c . As expected for conventional liquids with, e.g., Lennard-Jones interactions, the glass transition can occur either upon cooling or upon compression. This part of the transition line extends up to densities where φ exceeds φ_c^{HSS} , since the bonding effects due to the attraction stabilize the liquid phase. For large temperatures, the effects of the attraction get suppressed. Therefore, there exists a high-temperature piece of the transition line, where θ_c decreases with increasing φ_c . There appears a regime of high density, where the liquid can transform to a glass either by cooling or by heating. The possibility of such a reentry phenomenon is characteristic for systems with a hard-core repulsion. In a conventional system, the effect cannot occur, since a soft-core repulsion implies a decrease of the effective repulsion-core diameter with heating; and this decrease overcompensates the effect of the decrease of the effective attraction strength.

For $\delta < \delta^*$, the two mentioned transition-line parts no longer join smoothly. Rather the low-temperature line terminates the high-temperature one at some crossing-point, such that they appear as two separate transition lines. At very high temperature, the mechanism of glass formation is similar to the one of the HSS, and in general, the temperature dependence of the high-temperature transition line is weak. Glass transitions across this line are caused by an arrest of density fluctuations on the length scale of the inter-particle distance. A tagged particle is localized due to repulsion by its cage-forming neighbours. In contrast, the low-temperature line describes glass formation due to the arrest of density fluctuations on a length scale of the order of the attraction-shell width. Here, tagged particles are localized due to a formation of short bonds with their cage-forming neighbours. The density dependence of these transition points is weak, and the transition line extends into the regime of gel formation at low densities. On the high-density side, it extends into the glass regime, until it ends at an A_3 -glass-transition singularity, as indicated by the open circles in Fig. 5b.

Between the mentioned line-crossing point and the endpoint of the second transition line, there is a line of

glass-glass transitions. The averaged equilibrium structure, as characterized by the structure factor S_q , is the same on either side of this line. But the two different localization mechanisms imply qualitatively different frozen structures, reflected by differences in the Debye-Waller factor f_q . The one on the high-temperature side, shown by the uppermost solid line in Fig. 8, is similar to the Debye-Waller factor of the HSS at the same density. It exhibits a pronounced peak near the position q_0 of the structure-factor peak, and the zero-wave number limit f_0^c is about 0.7. On the low-temperature side, f_q^c is much larger, as is shown by the lowest of the dashed lines in Fig. 8. In particular, f_0^c is considerably increased. The f_q^c -versus- q curve for the attraction-dominated glass is bell-shaped like a Mößbauer-Lamb factor. The increase of f_0^c towards the upper limit unity is connected with a large enhancement of the longitudinal modulus. Crossing the glass-glass transition line, the longitudinal modulus as well as the shear modulus experiences a large discontinuity, as shown in Fig. 9. The large differences in the macroscopic elastic properties are the most obvious manifestations of the two localization mechanisms in the high-density system predicted by our theory.

Two general MCT predictions for the relaxation near a critical temperature or critical density have been confirmed by many experiments and molecular-dynamics simulations [54]. First, the structural relaxation exhibits a two-step scenario. Outside the transient, there occurs a relaxation towards the plateau f_q^c . For this step, $d^2\phi_q(t)/d(\ln t)^2$ is positive. Then there is the α process dealing with the relaxation from the plateau to zero. Its initial part exhibits a negative second derivative of the $\phi_q(t)$ -versus- $\ln t$ curve. Second, there holds the superposition principle for the α process. On a time window that expands with increasing relaxation time, the $\phi_q(t)$ -versus- $\ln t$ curves can be collapsed on a common master curve by shifts along the abscissa. These two simple results, which are fingerprints of the A_2 bifurcation, are not valid for the relaxation at states close to an A_4 singularity. The curves in Fig. 11 cannot be rescaled onto an α -relaxation master curve. The results in Fig. 12 do not exhibit changes of the second derivatives for $\phi_q(t)$ near the plateau f_q^c . It was shown that the higher-order glass-transition singularities A_3 and A_4 cause strong perturbations of the asymptotic laws usually considered, valid close to the A_2 bifurcation. In the present case, they can only be observed in windows, that might be outside the regimes accessible by experiments. In addition, the known asymptotic laws for the relaxation near A_3 or A_4 glass-transition singularities also show up only in windows, that are irrelevant for experimental studies. These predictions of our theory do not seem to be a peculiarity of the square-well system. Similar results already hold for simple one-component schematic models [52].

An exception to the findings summarized in the preceding paragraph is the logarithmic-decay law, Eq. (27). This characteristic feature of the dynamics near higher-

order glass-transition singularities could be identified easily in our results, as shown in Fig. 12. Indeed, it is shown in Fig. 11, that this $\ln t$ decay is a precursor phenomenon, hindering the evolution of the A_2 asymptotics. In particular, there can be a crossover from the $\ln t$ decay to the von-Schweidler decay around the point, where the $\phi_q(t)$ -versus- $\ln t$ curve crosses the plateau f_q^c , as is shown by curve 3 in Fig. 11. A similar scenario was recently observed for relaxation in a micellar system [55].

The found extreme stretching phenomena have important implications for the experimental tests of MCT. In an experiment, it is not easily possible to measure self-averaged correlation functions for states like the ones discussed in Fig. 12. Thus, experimental results are likely to refer to history-dependent non-equilibrium states, and ageing effects are likely to be more pronounced than they are for the normal liquid-glass transition. Even if proper averaging could be achieved, one cannot determine the Debye-Waller factor $f_q = \phi_q(t \rightarrow \infty)$ within accessible time windows, if the states are similar to the ones shown with labels 3 and 4 in Fig. 10. Similar conclusions apply for the measurements of the moduli near the glass-glass-transition line.

The presented theory is based on some assumptions which we would like to discuss in more detail. First, one should expect that the equilibrium state of the system in the density regime considered is a crystal rather than the assumed amorphous phase. In experiments for colloids, crystallization is bypassed by choosing a polydispersity p for the particle diameters. Since nucleation rates decrease dramatically with increasing p , a choice of p of some percent is sufficient to establish a metastable amorphous state for practically arbitrarily long times. A small p causes only small changes of the calculated structure factors, and thus only small changes in the coupling coefficients entering the MCT equations. Hence a small p will only imply small changes of the presented results. Indeed, it was shown for the HSS, that a change of p did not yield detectable changes of the measured $\phi_q(t)$ [56,57]. But, it is unclear how strongly, e.g., the calculated value δ^* for the attraction-well width at the A_4 singularity will change, if a realistic value for p is considered.

The structure factor S_q of the stable or metastable equilibrium is used as input information for our work. Thus, the second source of reservations is due to the errors hidden in the used S_q . A well-known problem is that of the so-called thermodynamic inconsistency. Thermodynamic quantities calculated along different routes using an approximate S_q as input often are not consistent with each other. Sophisticated closures involving adjustable parameters could be used to overcome this problem [4]. Alas, since thermodynamics deals with the $q \rightarrow 0$ limit, for which the phase volume in the mode-coupling integrals becomes small, one would gain no further insight carrying out our calculations of Secs. III and IV using an improved closure for S_q . For the HSS, one finds only minor changes in the numerical values for the

transition points [52,58], and the same is anticipated for the SWS. A further difficulty arises regarding the small- r limit of $c(r)$ and $g(r)$. Due to the approximations introduced for $Q(r)$, one cannot guarantee that the excluded-volume effect, $g(r < d) = 0$, is exactly reproduced. In fact, we find that $c(r)$ and thus $g(r)$ develop a pole A/r , cf. Eq. (12). Since $g(r)$ is a distribution and since A/r is integrable in three dimensions, an A/r -term is to be viewed as small, provided A is small. In the original work on the sticky hard spheres [27], $A = \mathcal{O}(K^2\varphi)$. In our solution, $A = \mathcal{O}(K\delta\varphi)$. The limits $r \rightarrow 0$ and $\delta \rightarrow 0$ do not commute, and our analytical solution decreases the error from a δ^0 to a δ^1 effect. Since our results based on the Percus-Yevick closure and on the mean-spherical approximation are in semi-quantitative agreement, we anticipate that better theories for S_q will not change the qualitative results of our theory.

Third, the range of applicability of the MCT is not understood. One can use the successful tests of the theory by the experiments performed on hard-sphere colloids, that were cited in Sec. I, as an *a posteriori* justification of MCT. But it is not clear, whether or not this theory can handle the effects caused by the formation of strong short bonds. On the other hand, the phenomenon of liquid stabilization due to bond formation and the resulting reentry effect, as well as the drastic changes of the elastic properties at the glass-glass transition, seem very plausible. The fact that MCT brings out these subtleties might be considered as an argument in favour of this approach. In summary, it is the intention of this paper to point out the possibility of new features of glassy dynamics and to suggest a search for these features by experiments on colloids.

ACKNOWLEDGMENTS

The work of F.S. and P.T. is supported by PRIN97-MURST and PRA-HOP-INFM, the work of M.F. by the Deutsche Forschungsgemeinschaft grant Fu 309/3, and the work of Th.V. by Verbundprojekt BMBF 03-G05TUM.

-
- [1] W. B. Russel, D. A. Saville, and W. R. Schowalter, *Colloidal Dispersions* (Cambridge University Press, New York, 1989).
- [2] P. N. Pusey, in *Liquids, Freezing and Glass Transition*, edited by J.-P. Hansen, D. Levesque, and J. Zinn-Justin (North-Holland, Amsterdam, 1991), p. 763.
- [3] W. C. K. Poon, *Cur. Opinion Colloid & Interf. Sci.* **3**, 593 (1998).
- [4] J. P. Hansen and I. R. McDonald, *Theory of Simple Liquids* (Academic Press, London, 1986).
- [5] U. Balucani and M. Zoppi, *Dynamics of the Liquid State* (Clarendon Press, Oxford, 1994).
- [6] W. van Meegen and P. N. Pusey, *Phys. Rev. A* **43**, 5429 (1991).
- [7] S. F. Edwards and P. W. Anderson, *J. Phys. F* **5**, 965 (1975).
- [8] W. van Meegen, S. M. Underwood, and P. N. Pusey, *Phys. Rev. Lett.* **67**, 1586 (1991).
- [9] W. van Meegen and S. M. Underwood, *Phys. Rev. Lett.* **70**, 2766 (1993).
- [10] W. van Meegen and S. M. Underwood, *Phys. Rev. E* **47**, 248 (1993).
- [11] W. van Meegen and S. Underwood, *Phys. Rev. Lett.* **72**, 1773 (1994).
- [12] W. van Meegen and S. M. Underwood, *Phys. Rev. E* **49**, 4206 (1994).
- [13] W. van Meegen, T. C. Mortensen, J. Müller, and S. R. Williams, *Phys. Rev. E* **58**, 6073 (1998).
- [14] U. Bengtzelius, W. Götze, and A. Sjölander, *J. Phys. C* **17**, 5915 (1984).
- [15] E. Leutheusser, *Phys. Rev. A* **29**, 2765 (1984).
- [16] W. Götze and L. Sjögren, *Rep. Prog. Phys.* **55**, 241 (1992).
- [17] W. van Meegen, *Transp. Theory Stat. Phys.* **24**, 1017 (1995).
- [18] T. G. Mason and D. A. Weitz, *Phys. Rev. Lett.* **75**, 2770 (1995).
- [19] E. Bartsch, M. Antonietti, W. Schupp, and H. Sillescu, *J. Chem. Phys.* **97**, 3950 (1992).
- [20] E. Bartsch, V. Frenz, S. Müller, and H. Sillescu, *Physica A* **201**, 363 (1993).
- [21] E. Bartsch, *J. Non-Cryst. Solids* **192-193**, 384 (1995).
- [22] E. Bartsch and V. Frenz and J. Baschnagel, *J. Chem. Phys.* **106**, 3743 (1997).
- [23] Ch. Beck, W. Härtl, and R. Hempelmann, *J. Chem. Phys.* **111**, 8209 (1999).
- [24] L. Fabbian, W. Götze, F. Sciortino, P. Tartaglia, and F. Thiery, *Phys. Rev. E* **59**, R1347 (1999); **60**, 2430 (1999).
- [25] J. Bergenholtz and M. Fuchs, *Phys. Rev. E* **59**, 5706 (1999).
- [26] G. Foffi, E. Zaccarelli, F. Sciortino, P. Tartaglia, and K. A. Dawson, *J. Stat. Phys.* (to be published).
- [27] R. J. Baxter, *J. Chem. Phys.* **49**, 2770 (1968); in *Physical Chemistry. An Advanced Treatise*, vol. VIIIA, edited by D. Henderson (Academic Press, New York, 1971), p. 267.
- [28] W. C. K. Poon, J. S. Selfe, M. B. Robertson, S. M. Ilett, A. D. Pirie, and P. N. Pusey, *J. Phys. II France* **3**, 1075 (1992).
- [29] H. N. W. Lekkerkerker, W. C. K. Poon, P. N. Pusey, A. Stroobants, and P. B. Warren, *Europhys. Lett.* **20**, 559 (1992).
- [30] A. Meller, T. Gisler, D. A. Weitz, and J. Stavans, *Langmuir* **15**, 1918 (1999).
- [31] M. C. Grant and W. B. Russel, *Phys. Rev. E* **47**, 2606 (1993).
- [32] H. Verduin and J. K. G. Dhont, *J. Colloid Interface Sci.* **172**, 425 (1995).
- [33] C. J. Rueb and C. F. Zukoski, *J. Rheology* **41**, 197 (1997).
- [34] C. J. Rueb and C. F. Zukoski, *J. Rheology* **42**, 1451

- (1998).
- [35] L. Lobry, N. Micali, F. Mallamace, C. Liao, and S.-H. Chen, Phys. Rev. E **60**, 7076 (1999).
- [36] W. G. T. Kranendonk and D. Frenkel, Mol. Phys. **64**, 403 (1988).
- [37] A. Lang, G. Kahl, C. N. Likos, H. Löwen, and M. Watzlawek, J. Phys.: Condens. Matter **11**, 10143 (1999).
- [38] R. J. Baxter, Aust. J. Phys. **21**, 563 (1968).
- [39] I. Nezbeda, Czech. J. Phys. B **24**, 703 (1974).
- [40] I. Nezbeda, Czech. J. Phys. B **27**, 247 (1977).
- [41] T. Franosch, M. Fuchs, W. Götze, M. R. Mayr, and A. P. Singh, Phys. Rev. E **55**, 7153 (1997).
- [42] W. Götze, in *Liquids, Freezing and Glass Transition*, edited by J.-P. Hansen, D. Levesque, and J. Zinn-Justin (North-Holland, Amsterdam, 1991), p. 287.
- [43] W. Götze and L. Sjögren, J. Math. Analysis and Appl. **195**, 230 (1995).
- [44] V. I. Arnol'd, *Catastrophe Theory* (Springer, Berlin, 1992).
- [45] M. Fuchs, W. Götze, and M. R. Mayr, Phys. Rev. E **58**, 3384 (1998).
- [46] J. Bergenholtz, M. Fuchs, and Th. Voigtmann, J. Phys. Condens. Matter **12**, 6575 (2000).
- [47] J. Bergenholtz and M. Fuchs, J. Phys. Condens. Matter **11**, 10171 (1999).
- [48] T. Franosch, W. Götze, M. R. Mayr, and A. P. Singh, J. Non-Cryst. Solids **235–237**, 71 (1998).
- [49] M. Fuchs and Th. Voigtmann, Philos. Mag. B **79**, 1799 (1999).
- [50] M. Fuchs and M. R. Mayr, Phys. Rev. E **60**, 5742 (1999).
- [51] W. Götze and L. Sjögren, J. Phys.: Condens. Matter **1**, 4203 (1989).
- [52] M. Sperl, Diploma thesis, Technische Universität München (2000).
- [53] W. Götze and R. Haussmann, Z. Phys. B **72**, 403 (1988).
- [54] W. Götze, J. Phys.: Condens. Matter **11**, A1 (1999).
- [55] F. Mallamace, P. Gambadauro, N. Micali, P. Tartaglia, C. Liao, and S.-H. Chen, Phys. Rev. Lett. **84**, 5431 (2000).
- [56] S. I. Henderson, T. C. Mortensen, G. M. Underwood, and W. van Megen, Physica A **233**, 102 (1996).
- [57] S. I. Henderson and W. van Megen, Phys. Rev. Lett. **80**, 877 (1998).
- [58] J.-L. Barrat, W. Götze, and A. Latz, J. Phys.: Condens. Matter **1**, 7163 (1989).

APPENDIX A: THE MSA FACTOR FUNCTION

1. General Formulae

Starting from Eqs. (4) and (5), Eq. (9) for the factor function, and expressions Eq. (10) and Eq. (11) for the parameters a , b , c shall be derived. The region $0 < r < 1 + \delta$, for which $Q(r)$ is nonzero, can be split into three parts:

$$Q(r) = \begin{cases} q_{\text{I}}(r), & 0 < r < \delta \\ q_{\text{II}}(r), & \delta < r < 1 \\ q_{\text{III}}(r'), & 0 < r' = r - 1 < \delta. \end{cases} \quad (\text{A1})$$

$Q(r)$ is continuous at the boundaries of the intervals, in particular $Q(1 + \delta) = 0$. From Eq. (5) together with $g(r) = 1 + h(r)$ and $G(r') = (1 + r')g(1 + r')$ the derivatives for the three parts of the factor function are obtained

$$q'_{\text{I}}(r) = ar + b - 12\varphi \int_r^\delta ds G(s - r)q_{\text{III}}(s), \quad (\text{A2a})$$

$$q'_{\text{II}}(r) = ar + b, \quad (\text{A2b})$$

$$q'_{\text{III}}(r') = ar + b - G(r') + 12\varphi \int_0^{r'} ds G(r' - s)q_{\text{I}}(s). \quad (\text{A2c})$$

Here $g(r) = 0$ for $0 < r < 1$ was used, and the definition for a and b is given in Eq. (6b). The integrated form of Eq. (4) is used to introduce the MSA closure as in Eq. (8),

$$q_{\text{III}}(r') = 12\varphi \int_{r'}^\delta ds q_{\text{III}}(s)q_{\text{I}}(s - r') + K \left[1 - \frac{r'}{\delta} + \frac{\delta}{2} \left(1 - \frac{r'^2}{\delta^2} \right) \right], \quad (\text{A3})$$

where $K = u_0\delta/k_B T$. In the following, Eqs. (A2) and (A3) are solved together with the reformulated expressions for a and b

$$a = 1 - 12\varphi \left[\int_0^\delta ds q_{\text{I}}(s) + \int_\delta^1 ds q_{\text{II}}(s) + \int_0^\delta ds q_{\text{III}}(s) \right], \quad (\text{A4a})$$

$$b = 12\varphi \left[\int_0^\delta ds s q_{\text{I}}(s) + \int_\delta^1 ds s q_{\text{II}}(s) + \int_0^\delta ds s q_{\text{III}}(s) + \int_0^\delta ds q_{\text{III}}(s) \right]. \quad (\text{A4b})$$

Equation (A2b) gives Eq. (9a),

$$q_{\text{II}}(r) = ar^2/2 + br + c, \quad (\text{A5})$$

where the continuity $q_{\text{II}}(r = 1) = q_{\text{III}}(r' = 0)$ yields c . For intervals I and III an expansion in δ for fixed K will be performed.

2. Leading Order

In Eq. (A3), r'/δ is of order δ^0 and the integral is of higher order, δ^1 . Therefore, in leading order,

$$q_{\text{III}}(r') = K(1 - r'/\delta). \quad (\text{A6})$$

The boundary condition mentioned above fixes $c = K - a/2 - b$ in leading order. Substituting Eq. (A6) into Eq. (A2c) and keeping only terms in lowest order in δ results in $G(r') = K/\delta$. The integral in Eq. (A2a) is

again of higher order and the continuity at the boundary $r = \delta$ gives the parabola also for region I,

$$q_{\text{I}}(r) = ar^2/2 + br + c. \quad (\text{A7})$$

Inserting the factor function into Eq. (A4) and keeping only lowest order terms, linear equations for the parameters are obtained

$$a = 1 - 12\varphi(a/6 + b/2 + c), \quad (\text{A8a})$$

$$b = 12\varphi(a/8 + b/3 + c/2), \quad (\text{A8b})$$

which leads to Eq. (10).

3. Next-To-Leading Order

Substituting the leading order results into Eqs. (A2) and (A3) produces the next-to-leading order. Subtracting Eq. (A2b) from Eq. (A2a), the result for the interval I is given as the derivative

$$\begin{aligned} q'_{\text{I}}(r) - q'_{\text{II}}(r) &= -12\varphi \int_r^\delta ds K/\delta K(1-s/\delta) = \\ &= -6\varphi K^2 (1-r/\delta)^2, \end{aligned} \quad (\text{A9})$$

which is integrated to give the last term in Eq. (9b). In Eq. (A3), the entire last line has to be taken into account for the next-to-leading order. The integral reads

$$\begin{aligned} 12\varphi \int_{r'}^\delta ds q_{\text{III}}(s)q_{\text{I}}(s-r') &= \\ &= 6K\delta \cdot \varphi c_0 (1-r'/\delta)^2 + \mathcal{O}(\delta^2). \end{aligned} \quad (\text{A10})$$

Combining Eqs. (A3) and (A10) yields the expression for the next-to-leading order term for the factor function in the outer shell, Eq. (9c). The continuity at $r = 1$ introduces a modification of c from its leading order value c_0 ,

$$c = K - a/2 - b + \delta \cdot K/2 + 6\delta \cdot K\varphi c_0, \quad (\text{A11})$$

where a and b are given by inserting the factor functions into Eq. (A4),

$$a = 1 - 12\varphi(a/6 + b/2 + c + \delta \cdot K/2), \quad (\text{A12a})$$

$$b = 12\varphi(a/8 + b/3 + c/2 + \delta \cdot K/2). \quad (\text{A12b})$$

This yields Eqs. (9), (10), and (11).

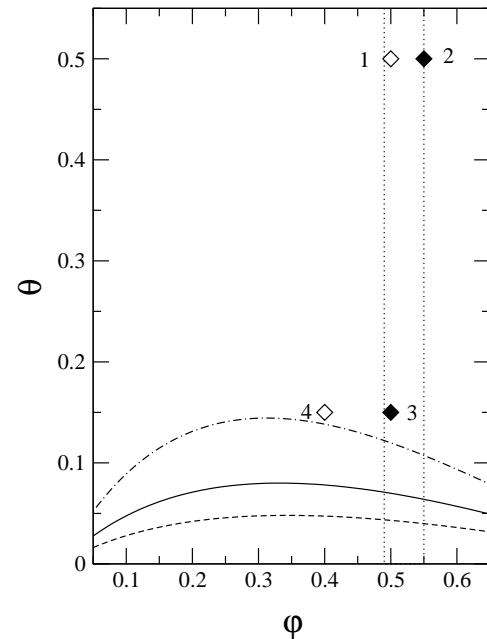


FIG. 1. Control-parameter plane for the square-well system (SWS), plotted as dimensionless temperature $\theta = k_B T/u_0$ versus packing fraction φ . The full line shows the spinodal calculated within the MSA for the relative attraction-well width $\delta = 0.05$. Dashed (dash-dotted) curves show the corresponding spinodals for $\delta = 0.03$ ($\delta = 0.09$). Vertical dotted lines mark the region for which the phase diagram is discussed below in Fig. 5. Diamonds mark the state parameters for which the structure factor is shown in Fig. 2.

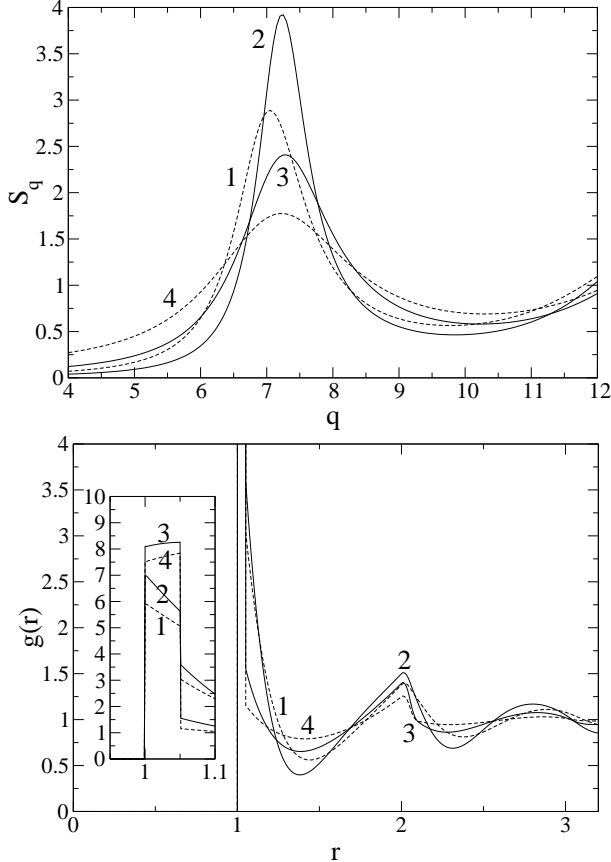


FIG. 2. Structure factor S_q and pair-correlation function $g(r)$ of the SWS calculated within the MSA for relative well width $\delta = 0.05$. The labels 1 to 4 correspond to the states indicated by the diamonds in Fig. 1. They are given by the pairs (φ, θ) of packing fraction and reduced temperature $(0.50, 0.50)$, $(0.55, 0.50)$, $(0.50, 0.15)$, and $(0.40, 0.15)$, respectively. Here and in the following figures, the hard core diameter is chosen as the unit of length, $d = 1$, and q is given here and in the following in units of d^{-1} .

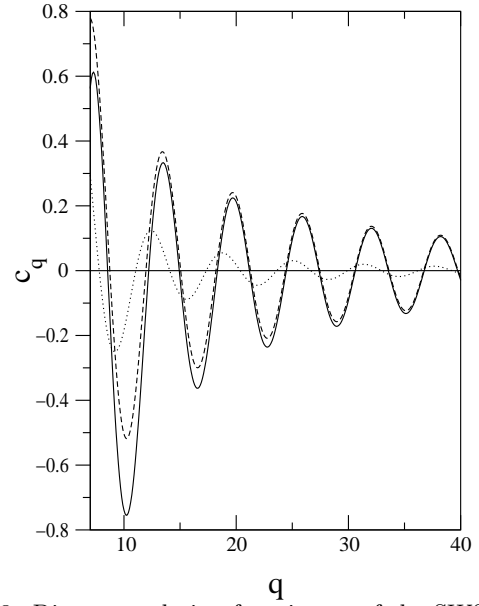


FIG. 3. Direct correlation function c_q of the SWS for relative well width $\delta = 0.05$, calculated within the MSA (solid line). Density and temperature are the ones considered in Figs. 1 and 2 for the label 3. The dashed line exhibits the leading asymptote c_q^{as} according to Eq. (12). The dotted line represents the same result with coefficient C replaced by zero (see text).

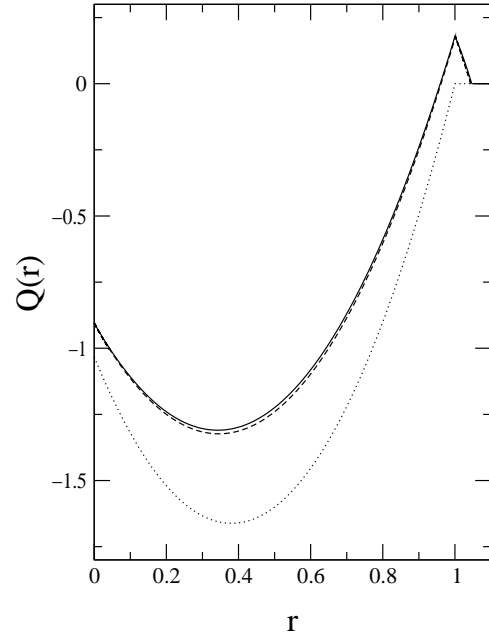


FIG. 4. Factor function $Q(r)$ of the SWS. The hard-core diameter is chosen as the unit of length. The dashed line is the PYA result for $\varphi = 0.5293$, reduced temperature $\theta = 1.10$, and well width parameter $\delta = 0.0429$. The full line is the MSA result for $\varphi = 0.5258$, $\theta = 0.2332$, $\delta = 0.0465$, chosen to represent the same physical state of interest in our discussion; see text for details. The dotted line shows the result for the HSS at packing fraction $\varphi = 0.516$.

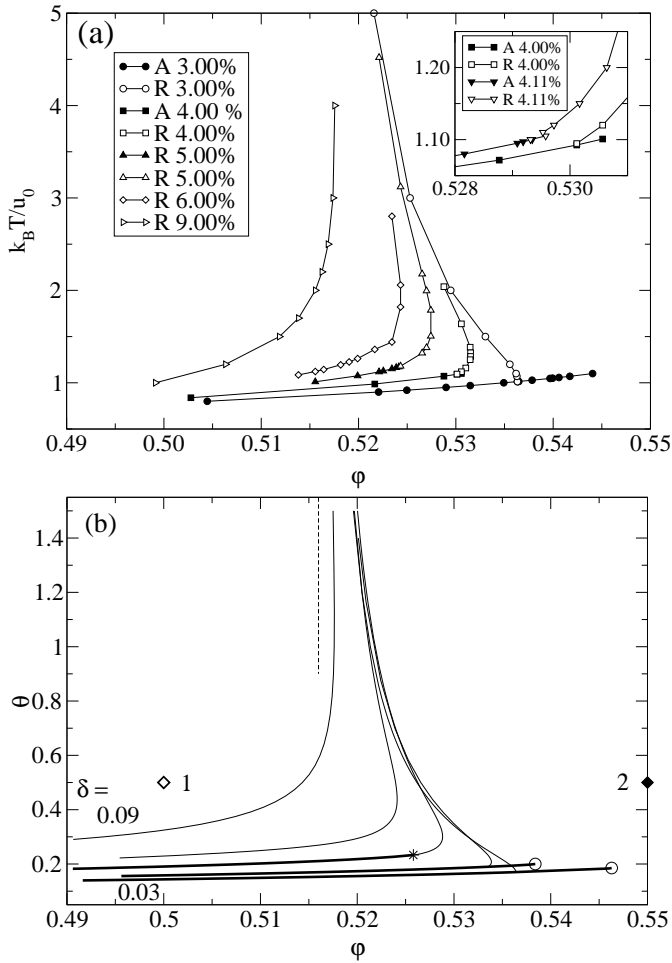


FIG. 5. The phase diagram of the SWS showing cuts through the control parameter space for fixed relative attraction-well width $\delta = \Delta/d$. The upper part (a) is based on the PYA for the structure factor S_q , and the ratio $\delta/(1 + \delta)$ is noted in the legend. The lower part (b) is based on the MSA for S_q , and the well widths are $\delta = 0.09, 0.06, 0.0465, 0.035$, and 0.03 , subsequently. The A_3 endpoints are marked by open circles and the A_4 by an asterisk. The vertical dashed line marks the transition line $\phi \approx 0.516$ for the hard-sphere system. For reference, states 1 and 2 from Fig. 1 are included as diamonds.

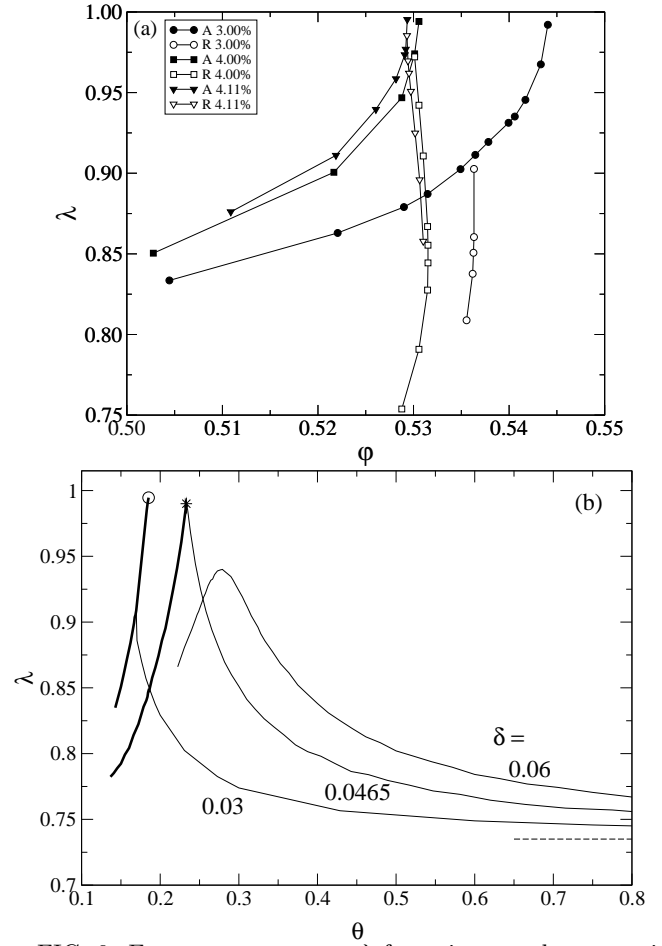


FIG. 6. Exponent parameter λ for points on three transition lines. The upper part (a) was calculated within the PYA for the ratios $\delta/(1 + \delta)$ noted in the legend. Part (b) shows the results for the MSA, where the dashed line indicates the value $\lambda = 0.735$ of the HSS.

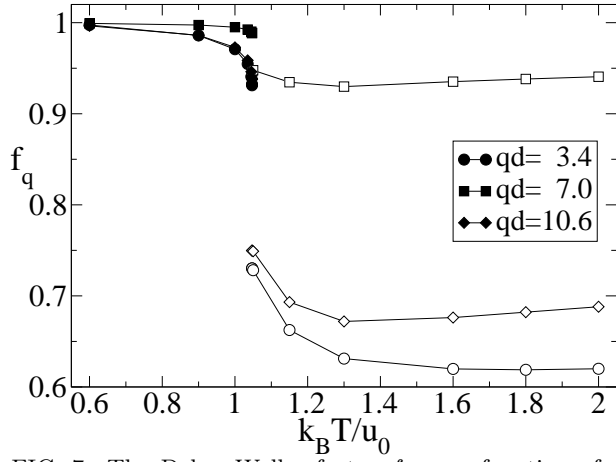


FIG. 7. The Debye-Waller factor f_q as a function of reduced temperature for fixed packing fraction $\varphi = 0.539672$ and fixed $\delta/(1 + \delta) = 0.03$. The wave vector $qd = 7.0$ is close to the structure factor peak position. The calculations are based on the PYA for S_q . The path through the parameter space deals with a glass-glass transition occurring at $\theta_c = 1.0471$, compare Fig. 5a.

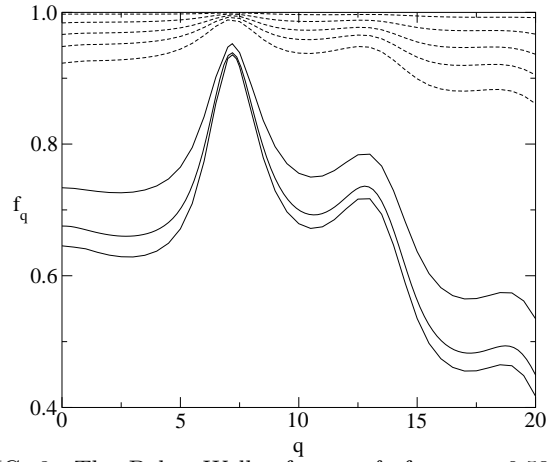


FIG. 8. The Debye-Waller factors f_q for $\varphi = 0.539672$, $\delta/(1 + \delta) = 0.03$. The temperature increases from top to bottom as $\theta = k_B T/u_0 = 0.600, 0.900, 1.000, 1.035, 1.0471$ (dashed lines) and $\theta = 1.047, 1.150, 1.300$ (full lines). The calculations are based on the PYA for S_q .

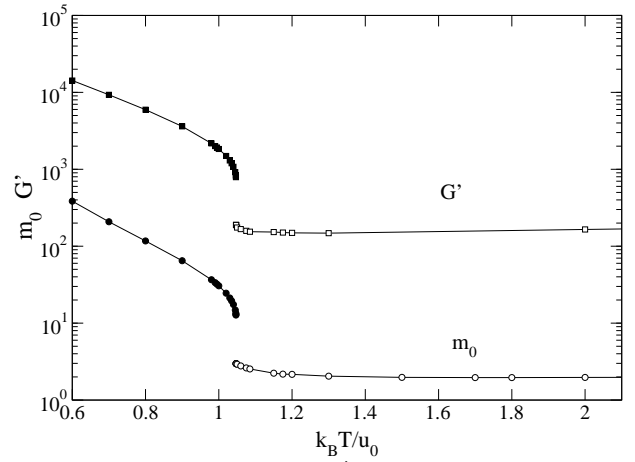


FIG. 9. The shear modulus G' and the dimensionless longitudinal elastic modulus m_0 as a function of the reduced temperature. The result is based on the PYA for S_q , and the parameters of state deal with the same path through the glass-glass transition as discussed in Figs. 7 and 8.

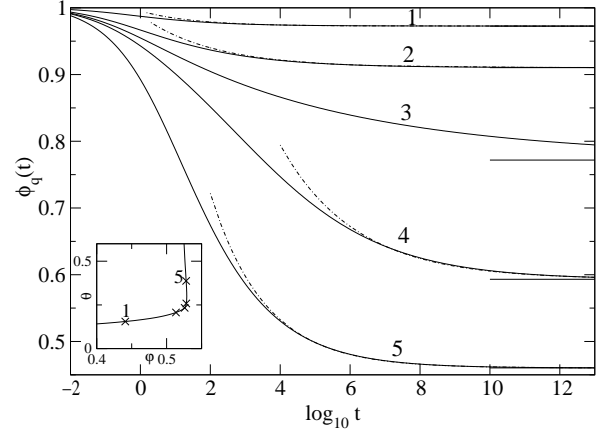


FIG. 10. The full lines are the critical correlators $\phi_q^c(t)$ for the wave vector $q = 4.2$ calculated with the MSA-structure factor for the critical attraction well width $\delta^* = 0.0465$. The states are located on the transition line as shown in the inset and refer to critical Debye-Waller factors $f_q^c = 0.973, 0.910, 0.772, 0.593, 0.460$ (from top to bottom as indicated by horizontal straight lines). For states 1 and 5, $\lambda = 0.80$ corresponding to a critical exponent $a = 0.279$; state 2 (4) refers to $\lambda = 0.895$ (0.908) corresponding to $a = 0.210$ (0.202). The dash-dotted lines show the asymptotes $f_q^c + A_q t^{-a}$. State 3 is at the A_4 singularity, given by Eq. (16b).

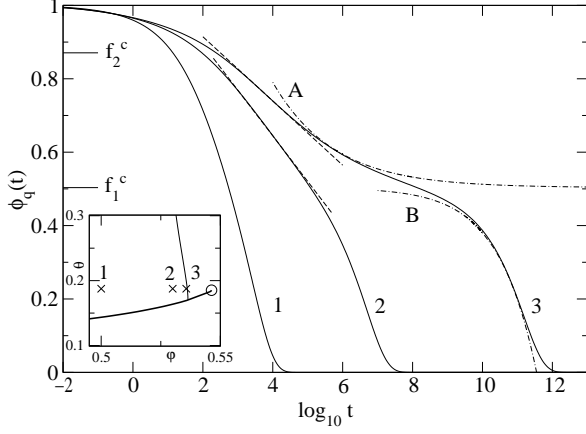


FIG. 11. Correlators $\Phi_q(t)$ for $q = 4.2$ calculated for the MSA-structure factor of a SWS with attraction-well width $\delta = 0.03$ and the reduced temperature $\theta = 0.1875$ for the three packing fractions $\varphi_1 = 0.5000$, $\varphi_2 = 0.5300$, $\varphi_3 = 0.5357$ (full lines). The inset shows the relevant section from the phase diagram of Fig. 5(b). The dashed-dotted lines with labels A and B exhibit the critical law $f_q^{(1)c} + A_q/t^{0.250}$ and the von-Schweidler law $f_q^{(1)c} - B_q t^{0.396}$, respectively. The straight dashed lines exhibit logarithmic decay laws, Eq. (27), see text.

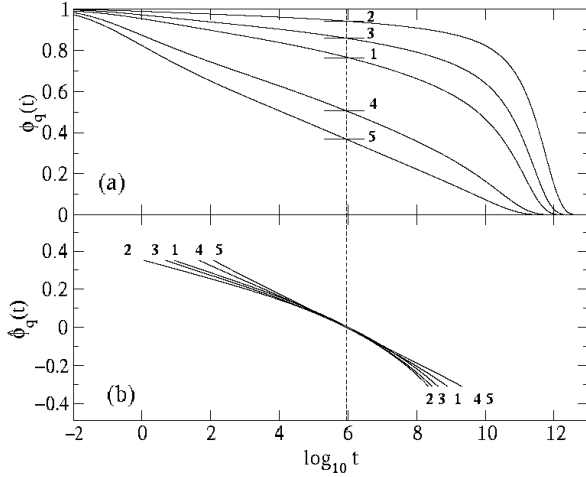


FIG. 12. Correlators for a liquid state close to the A_4 singularity calculated with the MSA for the structure factor. The curves in the upper panel (a) show the $\phi_q(t)$ where the labels 1 to 5 indicate the wave numbers $q = 4.2, 7.0, 8.2, 20.2, 24.2$. The corresponding critical Debye-Waller factors f_q^c are 0.764, 0.943, 0.860, 0.507, 0.369, respectively. The curves in the lower panel (b) exhibit the rescaled correlators $\hat{\phi}_q(t) = [\phi_q(t) - f_q^c]/h_q$. Here, the critical amplitudes $h_q = (1 - f_q^c)^2 e_q$ have the values 0.4665, 0.1343, 0.2881, 0.7291, 0.7835. The dashed vertical line marks the time $t_- = 8.9 \times 10^5$.